INTERNATIONAL JOURNAL FOR NUMERICAL METHODS IN FLUIDS, VOL. 21, 253–278 (1995)

ONE-DIMENSIONAL, TIME-DEPENDENT, HOMOGENEOUS, TWO-PHASE FLOW IN VOLCANIC CONDUITS

J. I. RAMOS

Departamento de Lenguajes y Ciencias de la Computación, E.T.S. Ingenieros Industriales, Universidad de Málaga, Plaza El Ejido, s/n, 29013-Málaga, Spain

SUMMARY

A one-dimensional, time-dependent, isothermal, homogeneous, two-phase flow model was developed to study magma ascent in volcanic conduits. The physical modeling equations were numerically solved by means of a TVD (total variation diminishing) predictor–corrector procedure and by means of a predictor–corrector technique based on the method of characteristics. The results from the transient model were verified with an analytical solution for wave propagation in conduits without friction and gravitational effects. The numerical solutions were also compared with those of a steady-state, homogeneous, two-phase model for basaltic and rhyolitic magma ascents in the fissures and circular conduits of Vesuvius and Mt St. Helens. An application of the model to magma decompression in conduits indicates very short times for gas exsolution, fragmentation, and shock wave propagation, implying that the modelling of gas exsolution should involve non-equilibrium kinetics effects. Future coupling of the transient magma ascent model with magma chamber and pyroclastic dispersion models should allow for more realistic simulations of the time-dependent behavior of real volcanic eruptions.

KEY WORDS: volcanic conduits; homogeneous flow; exsolution; total-variation-diminishing techniques; method of characteristics

1. INTRODUCTION

The flow of magma through a volcanic system to the ground surface takes place through various types of conduits depending on the magma at depth and on the geological and structural characteristics of the surrounding rocks and soil. Low viscosity or basaltic magmas erupt effusively from fissures, whereas the more viscous silicic magmas erupt pyroclastic products from central vents that may be fed by dikes or magma reservoirs. As the magma rises through conduits, both effusive and explosive eruptions exsolve the dissolved gases in the magma, and the magma may interact with aquifers within the volcanic system. The dissolved gases in magmas consist primarily of water vapour and carbon dioxide,[1] and the exsolved gases, in the form of bubbles, grow by mass diffusion, inertia, surface tension, heat transfer, and decompression.[2]

A large viscosity magma prevents the relative motion between the gas and the magma, and the two-phase flow along a conduit is essentially homogeneous until the gas concentration becomes sufficiently large and/or external perturbations cause magma fragmentation within the conduit.[3,4] Above the magma fragmentation level in a volcanic conduit, the flow consists of a continuous gas phase with dispersed pyroclasts, and a significant gas-particle velocity non-equilibrium may exist for large size pyroclasts. The flow of gas and magma through a volcanic conduit may also produce large differences between the lithostatic and magmatic pressures near the magma fragmentation level,[3] and these differences may cause rupture of the conduit wall. As a result, rock and water may flow into the

CCC 0271–2091/95/030253–26

Received 7 November 1994
Revised 13 February 1995

volcanic conduit leading to violent phreatomagmatic eruptions when vaporization of water with fragmented magma occurs.[4,5]

Previous models of gas-pyroclasts flows through volcanic conduits involved steady-state[3,6–12] and transient[13] approaches. The steady-state, non-homogeneous, two-phase flow model of gas-magma flow through volcanic conduits developed by Dobran[3] demonstrated the importance of magma composition and non-equilibrium slip flow in determining the eruption dynamics. This model was subsequently refined and used to study the plinian and pyroclastic flow eruption phases of Vesuvius in AD 79 and Mt St. Helens on 18 May 1980,[14,15] erosion processes in volcanic conduits,[16] and pyroclastic flow hazards at Vesuvius.[17]

Turcotte *et al.*[13] developed a transient, one-dimensional, homogeneous, two-phase flow model to study shock wave propagation along a volcanic conduit after a sudden pressure decrease in the magma and did not account for gravitational and frictional effects along the volcanic conduit. They showed that a sudden pressure decrease in the magma produces an exsolution front which propagates into the magma column, a fragmentation front which propagates into the air, and a shock wave which moves ahead of the fragmentation front. The transient model developed by Turcotte *et al.*[13] predicted exit velocities and magma fluxes which were found to be consistent with data from some typical eruptions.

An accurate model of explosive volcanic eruptions must involve unsteady motion of gas and magma through volcanic conduits. This unsteadiness is produced by the changing magma properties at the conduit inlet caused by the withdrawal of magma from temperature- and composition-stratified reservoirs,[18] water inflow into the conduits from underground aquifers,[19] changes in the conduit cross-section caused by erosion processes,[16] varying stress levels imposed on the conduit wall, and changes in the volcanic column dynamics above the volcanic vent.[20–22] For volcanic eruptions characterized by magma ascent times smaller than the times associated with the changes in the eruption dynamics (usually, Plinian eruptions), a quasi steady-state model of magma ascent may be acceptable. This is not so during the opening phases of eruptions and when the changes in the conduit cross-section are significant; these changes are caused, for example, by conduit wall collapses and activation and disactivation of aquifers at different depths. The Vulcanian eruptions[23] and the opening phases of Plinian eruptions resemble explosions[24] and require a transient magma ascent analysis.

The purpose of this paper is to present a one-dimensional, time-dependent, homogeneous, two-phase model for magma ascent in volcanic conduits of uniform cross-section in the absence of external magma–water interactions, but in the presence of gravitational and frictional effects. It will be shown that the results of the transient magma ascent model are in very good agreement with previous modelling approaches, and that the gravitational and frictional effects are important when modelling transient magma ascent along long volcanic conduits. Moreover, during the opening phases of magma decompression, very strong shock waves may propagate through the volcanic conduit, and the non-equilibrium kinetics effects associated with gas exsolution may be very important.

2. PHYSICAL MODEL

Figures 1 and 2 illustrate a volcanic conduit and the magma conditions at two different times. At time $t=0$ (Figure 1), magma under pressure is contained within a conduit at a height L_1 above the magma chamber. At $t=0^+$, the partition at $z=L_1$ is broken and the magma is allowed to decompress and push the air in front of it. At a subsequent time shown in Figure 2, the decompressing magma produces a downward moving exsolution front, an upward moving fragmentation front, and a shock wave in the air in front of the fragmentation front. The exsolution front corresponds to the pressure where the gases dissolved in the magma begin to exsolve and to a gas volumetric fraction $\alpha=0$, whereas the fragmentation front is assumed to correspond to $\alpha=0.75$.[2,3] The velocities of these fronts are denoted by u_s, u_f, respectively, while u_{sh} denotes the shock wave speed. D_H is the hydraulic diameter of the

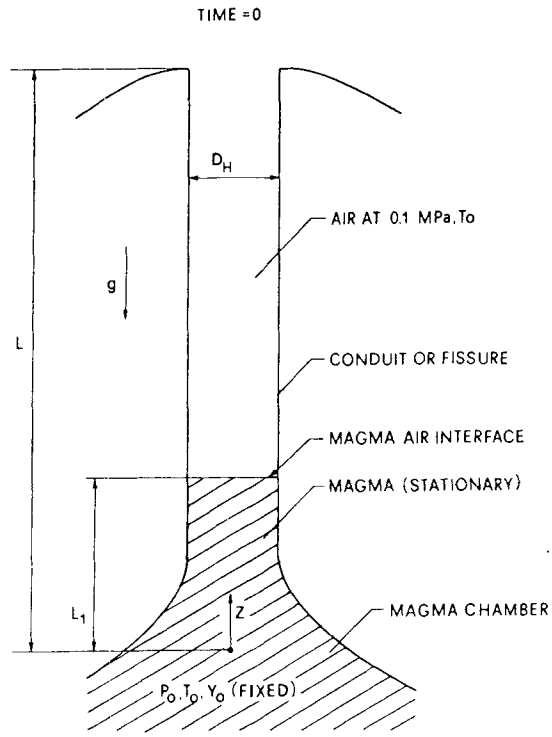

Figure 1. Schematic illustration of an initial state of magma in a volcanic conduit. Magma is kept under pressure at a height L_1 above the magma chamber

conduit, L is the conduit length, and the pressure P_0 and temperature T_0 of the magma in the magma chamber are assumed to be constant during decompression. It is also assumed that the magma flow is isothermal at the temperature T_0 which in the absence of magma–water interactions is an excellent assumption in view of the high thermal capacity of the magma which keeps the expansion of the gas nearly isothermal.[3,13] The air ahead of the shock wave is kept at atmospheric pressure and at the constant temperature of the magma.

The initial magma conditions illustrated in Figure 1 are idealized and only serve to establish some limiting conditions of magma ascent during the transient time of flow development leading to steady-state. In this state, the exsolution and fragmentation fronts are stationary and the flow exits into the atmosphere with pressure, velocity, and gas volumetric conditions determined by the conduit geometry, magma chamber pressure and temperature, dissolved water content in the magma, and atmospheric pressure. The opening phase of an eruption is extremely difficult to define due to the close interrelationship between the magma motion through opening fractures and thermal stress conditions of the non-homogeneous, non-isotropic surrounding rock media.[25]

2.1. Description of the physical model

The governing equations of one-dimensional, unsteady, two-phase, homogeneous fluid flow are[26]

$$\frac{\partial \rho}{\partial t} + \frac{\partial \rho u}{\partial z} = 0, \tag{1}$$

$$\frac{\partial \rho u}{\partial t} + \frac{\partial \rho u u}{\partial z} = -\frac{\partial P}{\partial z} - \rho g - \frac{1}{2}\frac{Per}{A}\rho f u|u|, \tag{2}$$

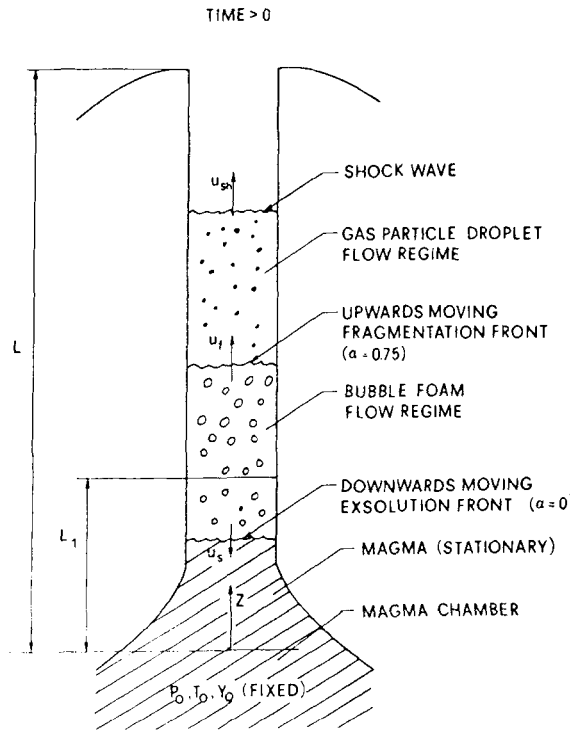

Figure 2. A sudden decompression of magma caused by the opening of the partition at L_1 produces a downward moving exsolution front and upward moving fragmentation and shock wave fronts as the magma expels the air from the volcanic conduit. The magma conditions at the conduit entrance are held fixed

where ρ is the mean density of the gas–magma mixture defined as

$$\rho = \alpha\rho_G + (1-\alpha)\rho_L, \tag{3}$$

u is the velocity component of the gas and magma along the volcanic conduit, P is the pressure, α is the volumetric or void fraction of the gas, f is the friction factor, t is time, z is the co-ordinate along the conduit, g is the gravitational acceleration, and *Per* and A are the perimeter and cross-sectional area of the conduit respectively. The subscripts G and L denote the gas and liquid, i.e. pyroclasts above the magma fragmentation level, and magma below this level, phases respectively.

The friction coefficient f can be specified as

$$f = \frac{a}{Re} + b, \qquad Re = \frac{\rho|u|D_H}{\mu}, \tag{4}$$

where a and b are constants, D_H is the conduit's hydraulic diameter, Re is the Reynolds number, and μ is the mixture viscosity.

The use of a mixture viscosity in evaluating the viscous drag at the wall is due to the fact that when bubbles or particles move through a fluid they distort the flow field and the motion of particles is affected by the forces exerted upon them by other particles. In the bubbly and gas-particle/droplet flow regimes, the mixture viscosity is given by[3]

$$\mu = \mu_L(1-\alpha)^{-2\cdot5(\mu_G+0\cdot4\mu_L)/(\mu_G+\mu_L)}, \quad 0 \leqslant \alpha \leqslant 0\cdot75, \tag{5}$$

$$\mu = \mu_G\left(1 - \frac{1-\alpha}{\alpha_{dm}}\right)^{-2\cdot5\alpha_{dm}(\mu_L+0\cdot4\mu_G)/(\mu_L+\mu_G)}, \quad 0\cdot75 < \alpha < 1, \tag{6}$$

where $\alpha_{dm} = 0\cdot62$ is the maximum particle packing density.

The gas can be modelled by an ideal equation of state,[3] and the exsolved gas mass fraction X can be expressed as

$$\rho_G = \frac{P}{\tilde{R}T_0}, \quad X = \left(1 + \frac{\rho_L}{\rho_G}\frac{1-\alpha}{\alpha}\right)^{-1}, \tag{7}$$

where $\tilde{R}$ is the specific gas constant and T_0 denotes the (constant) temperature.

The dissolved gas mass fraction, Y, may be determined from Henry's law from which the exsolved gas mass fraction can be found, i.e.

$$X = Y_0 - Y, \quad Y = SP^n, \tag{8}$$

where Y_0 is the maximum dissolved gas mass fraction in the magma, and S and n are exsolution constants which depend on the magma composition. It must be noted that Henry's law is an equilibrium equation which is strictly valid when the kinetics of interfacial mass transfer, i.e. exsolution, are much faster than the characteristic times of unsteadiness and residence of the flow in the volcanic conduit.

The above equations, together with the initial and boundary conditions to be specified in the next sections can be written in non-dimensional form by introducing the following variables and parameters

$$\tau = \frac{u_0 t}{D_H}, \quad \bar{z} = \frac{z}{D_H}, \quad \bar{u} = \frac{u}{u_0}, \quad \bar{\rho} = \frac{\rho}{\rho_a}, \quad \bar{\rho}_G = \frac{\rho_G}{\rho_a}, \tag{9}$$

$$\bar{\rho}_L = \frac{\rho_L}{\rho_a}, \quad \bar{P} = \frac{P}{P_{atm}}, \quad \bar{P}er = \frac{Per}{D_H}, \quad \bar{A} = \frac{A}{D_H^2},$$

where the reference velocity and density are defined, respectively, as

$$u_0 = \sqrt{\tilde{R}T_0}, \quad \rho_a = \frac{P_{atm}}{\tilde{R}T_0}. \tag{10}$$

The dimensionless form of the physical model expressed by (1)–(8) thus becomes

$$\frac{\partial \bar{\rho}}{\partial \tau} + \frac{\partial \bar{\rho}\bar{u}}{\partial \bar{z}} = 0, \tag{11}$$

$$\frac{\partial \bar{\rho}\bar{u}}{\partial \tau} + \frac{\partial \bar{\rho}\bar{u}\bar{u}}{\partial \bar{z}} = -\frac{\partial \bar{P}}{\partial \bar{z}} - \frac{\bar{\rho}}{Fr} - \frac{1}{2}\frac{\bar{P}er}{\bar{A}}\bar{\rho} f \bar{u}|\bar{u}|, \tag{12}$$

where

$$\bar{\rho} = \alpha\bar{\rho}_G + (1-\alpha)R, \quad R = \frac{\rho_L}{\rho_a}, \quad \bar{P} = \bar{\rho}_G, \quad X = \left(1 + \frac{R}{\bar{\rho}_G}\frac{1-\alpha}{\alpha}\right)^{-1} = Y_0 - Y, \tag{13}$$

$$f = \frac{a}{Re} + b, \quad Re = Re_0\frac{\bar{\rho}|\bar{u}|}{\bar{\mu}}, \quad \bar{\mu} = \frac{\mu}{\mu_0}, \quad Re_0 = \frac{\rho_a u_0 D_H}{\mu_0}, \quad Fr = \frac{u_0^2}{gD_H}, \tag{14}$$

where Fr is the Froude number.

The differential equations (11) and (12) can be solved for the density $\bar{\rho}$ and velocity $\bar{u}$ as a function of τ and $\bar{z}$, since the gas volumetric fraction, pressure, gas density, and exsolved gas mass fraction can be expressed in terms of the mixture density. To illustrate this procedure, it is convenient to express the dissolved gas mass fraction in a piecewise linear manner as a function of the pressure, i.e.

$$Y = \bar{\beta} - \gamma P = \bar{\beta} - \bar{\gamma}\bar{P}, \quad \bar{\gamma} = \gamma P_{atm}, \tag{15}$$

where $\bar{\beta}$ and γ are constants whose values depend on the interval used to approximate (8b) in the piecewise linear fashion defined by (15a).

Using (15) and (13), we have

$$\alpha = -\frac{\hat{\beta} - R}{2\hat{\gamma}} \pm \sqrt{\left(\frac{\hat{\beta} - R}{2\hat{\gamma}}\right)^2 - \frac{R - \bar{\rho}}{\hat{\gamma}}} \geq 0, \tag{16}$$

$$\bar{\rho}_G = \bar{P} = \frac{1}{\bar{\gamma}}\left(\bar{Y}_0 - (1-\alpha)\frac{R}{\bar{\rho}}\right), \tag{17}$$

where

$$\bar{Y}_0 = Y_0 - \bar{\beta}, \quad \hat{\beta} = \frac{1}{\bar{\gamma}}\left(1 - \bar{Y}_0 - \frac{R}{\bar{\rho}}\right), \quad \hat{\gamma} = \frac{R}{\bar{\rho}\bar{\gamma}}. \tag{18}$$

2.2. *Initial conditions*

The solution of (11) and (12) requires initial and boundary conditions. The initial conditions shown in Figure 1 define stationary magma and air in the volcanic conduit where the gas in the magma is assumed to be completely dissolved. Thus, for $\bar{z} \leqslant L_1/D_H$,

$$\bar{u}(\tau = 0, \bar{z}) = 0, \quad \bar{\rho}(\tau = 0, \bar{z}) = R, \tag{19}$$

and

$$\alpha(\tau = 0, \bar{z}) = X(\tau = 0, \bar{z}) = 0, \quad \bar{P}(\tau = 0, \bar{z}) = \frac{P_0}{P_{atm}} - \frac{\rho_L g L_1}{P_{atm}} \frac{D_H}{L_1}\bar{z}. \tag{20}$$

For $\bar{z} > L_1/D_H$, the air in the volcanic conduit is stationary and the pressure is hydrostatic at temperature T_0.

2.3. *Boundary conditions*

The boundary conditions at $\bar{z} = 0$ and $\bar{z} = L/D_H$ must be determined from (11) and (12) as follows. Equations (11) and (12) can be as

$$\frac{\partial \mathbf{U}}{\partial \tau} + \frac{\partial \mathbf{F}}{\partial \bar{z}} = \mathbf{S}, \tag{21}$$

where the vectors **U**, **F**, and **S** are defined as

$$\mathbf{U} = \begin{pmatrix} U_1 \\ U_2 \end{pmatrix} = \begin{pmatrix} \bar{\rho} \\ \bar{\rho}\bar{u} \end{pmatrix}, \tag{22}$$

$$\mathbf{F} = \begin{pmatrix} F_1 \\ F_2 \end{pmatrix} = \begin{pmatrix} \bar{\rho}\bar{u} \\ \bar{\rho}\bar{u}\bar{u} + \bar{P} \end{pmatrix}, \tag{23}$$

$$\mathbf{S} = \begin{pmatrix} S_1 \\ S_2 \end{pmatrix} = \begin{pmatrix} 0 \\ -\dfrac{\bar{\rho}}{Fr} - \dfrac{1}{2}\dfrac{\bar{P}er}{A}\bar{\rho} f \bar{u}|\bar{u}| \end{pmatrix}. \tag{24}$$

Equation (21) can also be written as

$$\frac{\partial \mathbf{U}}{\partial \tau} + \mathbf{H}\frac{\partial \mathbf{U}}{\partial z} = \mathbf{S}, \tag{25}$$

where $\mathbf{H} = \partial \mathbf{F}/\partial U$ is a Jacobian matrix whose eigenvalues and eigenvectors are, respectively,

$$\lambda_+ = \bar{u} + \bar{c}, \quad \lambda_- = -\bar{u} + \bar{c}, \tag{26}$$

$$(1, \lambda_+)^{\mathrm{T}}, \quad (1, \lambda_-)^{\mathrm{T}}, \tag{27}$$

the superscript T denotes transpose and $\bar{c}^2 = \partial \bar{P}/\partial \bar{\rho}$ is the square of the speed of sound. Therefore, (25) is hyperbolic and the boundary conditions at $\bar{z} = 0$ and $\bar{z} = L/D_{\mathrm{H}}$ here referred to as inflow and outflow, respectively, are determined from the number of characteristics entering into the flow field at these boundaries. Since the flow Mach number is less than one except at the outflow boundary where it may be equal to one, the number of incoming characteristics at the inflow boundary is one. Therefore, only one boundary condition may be specified at that boundary. An analogous reasoning at the outflow boundary indicates that only one boundary condition may be imposed there for subsonic, i.e. $|\bar{u}| < \bar{c}$, flow, and that no boundary condition may be imposed at the outflow boundary if the flow is choked at the exit of the volcanic conduit.

The following three types of inflow boundary conditions were employed in the numerical experiments reported in this paper

$$\bar{u}(\tau, \bar{z} = 0) = \bar{u}_0, \tag{28}$$

$$\bar{\rho}(\tau, \bar{z} = 0) = R, \tag{29}$$

$$\bar{P}(\tau, \bar{z} = 0) = P_0/P_{\mathrm{atm}}. \tag{30}$$

Equation (28) specifies the conduit inlet velocity $\bar{u}_0$ which may be determined from the mass eruption rate, conduit diameter, and magma density. Equation (29) corresponds to a gas volumetric or void fraction equal to zero (cf. (13a)) which implies (cf. (13d)) that the exsolved mass fraction at the entrance of the conduit is zero. Finally, (30) specifies the pressure at the conduit's entrance. If this pressure is above the exsolution pressure, $X = 0$, $\bar{\rho}_{\mathrm{G}} = 0$ and $\bar{\rho} = R$ according to (8), (7) and (3), respectively.

When the flow is not choked at the conduit exit, the exit pressure is atmospheric. For choked flows, the exit pressure must be determined from the model, and the flow velocity at the conduit exit is equal to the local speed of sound to prevent upstream propagation of the downstream pressure. A choked flow condition in a volcanic conduit corresponds to the maximum flow rate compatible with the conduit geometry, magma properties, and conduit flow inlet conditions under steady state conditions.[3] Thus,

$$\bar{P}(\tau, \bar{z} = L/D_H) = 1 \quad \text{(non-choked flow)}, \tag{31}$$

$$\bar{u}(\tau, \bar{z} = L/D_H) = \sqrt{\frac{\partial \bar{P}}{\partial \bar{\rho}}} \quad \text{(choked flow)}, \tag{32}$$

The nondimensional parameters of the homogeneous, two-phase flow model presented in this paper are Fr, $\bar{L} = L/D_{\mathrm{H}}$, $\bar{L}_1 = L_1/D_{\mathrm{H}}$, $\bar{P}er/\bar{A}$, friction coefficients a and b, Re_0, R, Y_0, μ_{G}/μ_0, P_0/P_{atm}, ρ_L gL_1/P_{atm}, and the local values of $\bar{\beta}$ and $\bar{\gamma}$.

3. NUMERICAL SOLUTION PROCEDURE

Equation (21) must be solved in the single- and two-phase regions of the conduit subject to the initial and boundary conditions specified in the previous section. In the single phase region of the conduit where the gas is completely dissolved in the magma, $\alpha = X = 0$, the magma density is assumed constant, and (21) becomes

$$\bar{\rho} = R, \quad \bar{u} = \text{const} = \bar{u}_0, \tag{33}$$

$$\bar{P} = \frac{P_0}{P_{\text{atm}}} - \left(\frac{R}{Fr} - \frac{1}{2} \frac{\bar{P}er}{\bar{A}} f R \bar{u}_0 |\bar{u}_0| \right) \bar{z}, \tag{34}$$

for

$$\bar{P} \geqslant \frac{\bar{\beta} - Y_0}{\bar{\gamma}}, \tag{35}$$

as determined from (15). When the equality holds in (35), the gas dissolved in the magma begins exsolving and the flow develops as a bubbly flow for $\alpha \leq 0{\cdot}75$ and as a gas-particle/droplet flow for $\alpha > 0{\cdot}75$.

Equation (21) was solved numerically by means of the techniques presented in the following subsections. For convenience, the bars over the dimensionless variables are dropped in what follows.

3.1. *Method of characteristics*

Equations (11) and (12) may be written as

$$\frac{\partial P}{\partial \tau} + u \frac{\partial P}{\partial z} + \rho c^2 \frac{\partial u}{\partial z} = 0, \tag{36}$$

$$\rho \left(\frac{\partial u}{\partial \tau} + u \frac{\partial u}{\partial z} \right) + \frac{\partial P}{\partial z} = -\frac{\rho}{Fr} - \frac{1}{2} \frac{Per}{A} \rho f u |u|, \tag{37}$$

where use has been made of the isothermal character of the flow.

Equations (36) and (37) can be combined as

$$\frac{\partial P}{\partial \tau} + (u + Q) \frac{\partial P}{\partial z} + \rho Q \left[\frac{\partial u}{\partial \tau} + \left(u + \frac{c^2}{Q} \right) \frac{\partial u}{\partial z} \right] = Q \left(-\frac{\rho}{Fr} - \frac{1}{2} \frac{Per}{A} \rho f u |u| \right), \tag{38}$$

where Q has been introduced arbitrarily.

If $Q = c$, i.e. along

$$\frac{\mathrm{d}z}{\mathrm{d}\tau} = \lambda_+ = u + c, \tag{39}$$

Equation (38) becomes

$$\frac{\partial P}{\partial \tau} + \lambda_+ \frac{\partial P^+}{\partial z} + \rho c \left(\frac{\partial u}{\partial \tau} + \lambda_+ \frac{\partial u^+}{\partial z} \right) = -c \left(\frac{\rho}{Fr} + \frac{1}{2} \frac{Per}{A} \rho f u |u| \right). \tag{40}$$

If $Q = -c$, i.e. along

$$\frac{\mathrm{d}z}{\mathrm{d}\tau} = \lambda_- = u - c, \tag{41}$$

Equation (38) becomes

$$\frac{\partial P}{\partial \tau} + \lambda_- \frac{\partial P^-}{\partial z} - \rho c \left(\frac{\partial u}{\partial \tau} + \lambda_- \frac{\partial u^-}{\partial z} \right) = c \left(\frac{\rho}{Fr} + \frac{1}{2} \frac{Per}{A} \rho f u |u| \right). \tag{42}$$

Adding (40) and (42), the following λ-form equation for the pressure results

$$\frac{\partial P}{\partial \tau} + \frac{1}{2} \left(\lambda_+ \frac{\partial P^+}{\partial z} + \lambda_- \frac{\partial P^-}{\partial z} \right) + \frac{1}{2} \rho c \left(\lambda_+ \frac{\partial u^+}{\partial z} - \lambda_- \frac{\partial u^-}{\partial z} \right) = 0. \tag{43}$$

Similarly, by subtracting (40) and (42), the following λ-form equation for the velocity is obtained

$$\frac{\partial u}{\partial \tau} + \frac{1}{2\rho c} \left(\lambda_+ \frac{\partial P^+}{\partial z} - \lambda_- \frac{\partial P^-}{\partial z} \right) + \frac{1}{2} \left(\lambda_+ \frac{\partial u^+}{\partial z} + \lambda_- \frac{\partial u^-}{\partial z} \right) = -\frac{1}{\rho} \left(\frac{\rho}{Fr} + \frac{1}{2} \frac{Per}{A} \rho f u |u| \right). \tag{44}$$

Note that, in (43) and (44), the spatial derivatives have been marked with + and − in order to indicate the characteristic directions along which these derivatives are approximated.

Equations (43) and (44) were solved by means of the following explicit, predictor–corrector method.[27]

Predictor step

This step consists of two parts. In the first part, the predicted solution is determined from

$$\mathbf{U}_i^* = \mathbf{U}_i^n + \Delta\tau \left(\frac{\partial \mathbf{U}}{\partial \tau} \right)_i^n, \tag{45}$$

where, for example,

$$\left(\frac{\partial P^+}{\partial z} \right)_i = \frac{P_i^n - P_{i-1}^n}{\Delta z}, \tag{46}$$

$$\left(\frac{\partial P^-}{\partial z} \right)_i = \frac{P_{i+1}^n - P_i^n}{\Delta z}. \tag{47}$$

In the second part, the predicted values of $\partial \mathbf{U}^*/\partial \tau$ are determined from (43) and (44) by means of the following expressions

$$\left(\frac{\partial P^+}{\partial z} \right)_i = \frac{2P_i^n - 3P_{i-1}^n + P_{i-2}^n}{\Delta z}, \tag{48}$$

$$\left(\frac{\partial P^-}{\partial z} \right)_i = \frac{-2P_i^n + 3P_{i+1}^n - P_{i+2}^n}{\Delta z}. \tag{49}$$

Corrector step

The corrected values of $\partial U/\partial \tau$, i.e. $\partial U^c/\partial \tau$, are determined from (43) and (44) with

$$\left(\frac{\partial P^+}{\partial z} \right)_i = \frac{P_i^* - P_{i-1}^*}{\Delta z}, \tag{50}$$

$$\left(\frac{\partial P^-}{\partial z} \right)_i = \frac{P_{i+1}^* - P_i^*}{\Delta z.} \tag{51}$$

Finally, $\mathbf{U}_i^{n+1}$ is calculated as

$$\mathbf{U}_i^{n+1} = \mathbf{U}_i^n + \frac{\Delta\tau}{2}\left(\left(\frac{\partial \mathbf{U}}{\partial \tau}\right)_i^c + \left(\frac{\partial \mathbf{U}}{\partial \tau}\right)_i^*\right) \tag{52}$$

The predictor–corrector method presented in this section is only applicable at the interior points. Boundary points require a special treatment as shown next.

Boundary conditions

The inflow and outflow boundary conditions were implemented as follows. Equation (38) with $Q = c$ becomes along the right running characteristic, i.e. $\eta = \text{const.}$, whose slope is given by (39)

$$\frac{dP}{d\eta} + \rho c \frac{du}{d\eta} = -c\left(\frac{\rho}{Fr} + \frac{1}{2}\frac{Per}{A}\rho f u|u|\right), \tag{53}$$

while the same equation becomes along the left running characteristic, i.e. $\xi = \text{const.}$, whose slope is given by (41)

$$\frac{dP}{d\xi} - \rho c \frac{du}{d\xi} = c\left(\frac{\rho}{Fr} + \frac{1}{2}\frac{Per}{A}\rho f u|u|\right). \tag{54}$$

Integration of (53) and (54) along the right and left, respectively, running characteristics yields

$$P_i^{n+1} - P_{i-1}^n + (\rho c)_{i-1}^n (u_i^{n+1} - u_{i-1}^n) = -\Delta\tau\left(c\left(\frac{\rho}{Fr} + \frac{1}{2}\frac{Per}{A}\rho f u|u|\right)\right)_{i-1}^n, \tag{55}$$

$$P_i^{n+1} - P_{i+1}^n + (\rho c)_{i+1}^n (u_i^{n+1} - u_{i+1}^n) = \Delta\tau\left(c\left(\frac{\rho}{Fr} + \frac{1}{2}\frac{Per}{A}\rho f u|u|\right)\right)_{i+1}^n, \tag{56}$$

where the coefficients of (53) and (54) have been evaluated at the known time level.

Equation (55) was solved simultaneously with the imposed atmospheric pressure at the outflow boundary if the exit flow was subsonic. Similarly, Equation (56) is solved simultaneously with the imposed boundary condition at the inflow boundary. If the flow is sonic at the outflow boundary, Equation (55) is to be solved subject to (32).

The method of characteristics presented in this section is explicit, second-order accurate, and non-conservative, and it is not capable of capturing accurately shock waves. It is related to flux splitting algorithms since the Jacobian matrix, $\mathbf{H}$, can be written as $\mathbf{H} = \mathbf{H}^+ + \mathbf{H}^-$ where $\mathbf{H}^+ = \mathbf{T}\Lambda^+\mathbf{T}^{-1}$ and $\mathbf{H}^- = \mathbf{T}\Lambda^-\mathbf{T}^{-1}$, $\mathbf{T}$ is the matrix of left eigenvectors associated with $\mathbf{H}$, and Λ^+ and Λ^- are the diagonal matrices of positive and negative eigenvalues of $\mathbf{H}$ respectively.[28] With this splitting,

$$\mathbf{H}\frac{\partial \mathbf{U}}{\partial z} = \mathbf{H}^+\frac{\partial \mathbf{U}}{\partial z} + \mathbf{H}^-\frac{\partial \mathbf{U}}{\partial z}$$

and the terms $\partial\mathbf{U}/\partial z$ which post-multiply $\mathbf{H}^+$ and $\mathbf{H}^-$ are discretized by means of backward and forward differences respectively. Flux splitting algorithms which use one-sided differences are capable of capturing shock waves, but they are less economical than the method of characteristics presented in this section.[29]

3.2. *TVD finite difference method*

Equation (21) was also solved by means of the explicit MacCormack's finite difference method[30] with the artificial viscosity model due to Davis[31] which yields a TVD (total variation diminishing)

technique. The MacCormack's finite difference method predicts the solution at time τ^{n+1}, i.e. $\mathbf{U}_i^p$, by means of the following first-order forward temporal and spatial difference expression

$$\mathbf{U}_i^p = \mathbf{U}_i^n - \frac{\Delta\tau}{\Delta z}(\mathbf{F}_{i+1}^n - \mathbf{F}_i^n), \tag{57}$$

while corrected solutions, i.e. $\mathbf{U}_i^c$, at the same time step are obtained by means of the following backward temporal and spatial difference expression

$$\mathbf{U}_i^c = \frac{1}{2}(\mathbf{U}_i^n + \mathbf{U}_i^p - \frac{\Delta\tau}{\Delta z}(\mathbf{F}_i^p - \mathbf{F}_{i-1}^p)). \tag{58}$$

MacCormack's finite difference scheme is conservative and consistent but produces oscillations near steep flow gradients unless artificial viscosity is employed to smooth the corrected solution. In this paper, the final solution at time τ^{n+1} was calculated as

$$\mathbf{U}_i^{n+1} = \mathbf{U}_i^c + \mathbf{D}_{i+\frac{1}{2}}^n - \mathbf{D}_{i-\frac{1}{2}}^n, \tag{59}$$

where the dissipative term $\mathbf{D}_{i+\frac{1}{2}}^n$ takes into account the relative changes in the solution gradients as

$$r_i^+ = \frac{(\Delta\mathbf{U}_{i-\frac{1}{2}}^n)^{\mathrm{T}}\Delta\mathbf{U}_{i+\frac{1}{2}}^n}{(\Delta\mathbf{U}_{i+\frac{1}{2}}^n)^{\mathrm{T}}\Delta\mathbf{U}_{i+\frac{1}{2}}^n}, \tag{60}$$

$$r_i^- = \frac{(\Delta\mathbf{U}_{i-\frac{1}{2}}^n)^{\mathrm{T}}\Delta\mathbf{U}_{i+\frac{1}{2}}^n}{(\Delta\mathbf{U}_{i-\frac{1}{2}}^n)^{\mathrm{T}}\Delta\mathbf{U}_{i-\frac{1}{2}}^n}, \tag{61}$$

where

$$\Delta\mathbf{U}_{i+\frac{1}{2}}^n = \mathbf{U}_{i+1}^n - \mathbf{U}_i^n. \tag{62}$$

A flux limiter, ϕ, was defined as

$$\phi(r_i^+, r_i^-) = \max(0, \min(2r_i^+, r_i^-, 1), \min(2r_i^-, r_i^+, 1)), \tag{63}$$

while the following Courant-number-dependent function, $C(v)$, was calculated as

$$C(v) = v(1 - v), \quad \text{if} \quad v \leq \tfrac{1}{2}, \tag{64}$$

$$C(v) = \frac{1}{4}, \quad \text{otherwise}, \tag{65}$$

where $v = \psi\Delta\tau/\Delta z$ and ψ denotes the largest eigenvalue of $\mathbf{H}$.

Finally, a dissipation coefficient, $K_{i+\frac{1}{2}}^n$, was calculated as

$$K_{i+\frac{1}{2}}^n(r_i^+, r_{i+1}^-) = \frac{1}{2}C(v)(1 - \phi(r_i^+, r_{i+1}^-)), \tag{66}$$

so that the dissipative term in (59) becomes

$$\mathbf{D}_{i+\frac{1}{2}}^n = K_{i+\frac{1}{2}}^n(r_i^+, r_{i+1}^-)\mathbf{U}_{i+\frac{1}{2}}^n. \tag{67}$$

The MacCormack's finite difference method is second-order accurate in both space and time, and conservative.

3.3. *The Lax–Wendroff method with smoothing*

Equation (21) was also solved numerically by means of the two-step, second-order accurate (in both space and time), predictor/corrector procedure of Lax–Wendroff[29] at each time step. This procedure introduces, however, unphysical oscillations due to dispersion errors near steep fronts. To eliminate these oscillations and maintain the positivity of the solution, smoothing was introduced after obtaining the solution of the corrector step.

The computational domain involved the entire conduit and consisted of uniformly spaced grid points along the conduit. Different number of points were used to ascertain the grid-independence of the numerical solution. For an interior node i and time step n, the predictor step is

$$\hat{\mathbf{U}}_{i+\frac{1}{2}} = \frac{1}{2}(\mathbf{U}_i^n + \mathbf{U}_{i+1}^n) - \frac{\Delta\tau}{\Delta\bar{z}}(\mathbf{F}_{i+1}^n - \mathbf{F}_i^n) + \Delta\tau\, \mathbf{S}_{i+\frac{1}{2}}^n, \tag{68}$$

where $\Delta\tau$ and $\Delta\bar{z}$ are the increments in time and space respectively. The corrector step is

$$\mathbf{U}_i^{n+1} = \mathbf{U}_i^n - \frac{\Delta\tau}{\Delta\bar{z}}(\hat{\mathbf{F}}_{i+\frac{1}{2}} - \hat{\mathbf{F}}_{i-\frac{1}{2}}) + \Delta\tau\, \hat{\mathbf{S}}_i, \tag{69}$$

The final solution is then obtained by applying smoothing to the dependent variables according to the following procedure

$$\begin{aligned}\mathbf{U}_i^{\text{smooth}} = \mathbf{U}_i^{n+1} + \nu\frac{\Delta\tau}{\Delta\bar{z}}(&|\mathbf{U}_{i+1}^{n+1} - \mathbf{U}_i^{n+1}|(\mathbf{U}_{i+1}^{n+1} - \mathbf{U}_i^{n+1}) \\ &- |\mathbf{U}_i^{n+1} - \mathbf{U}_{i-1}^{n+1}|(\mathbf{U}_i^{n+1} - \mathbf{U}_{i-1}^{n+1})),\end{aligned} \tag{70}$$

where ν is an artificial viscosity coefficient which is to be found on the basis of trial and error to avoid excessive smearing of the solution and oscillations in front of and behind steep flow gradients. A value of $\nu = 0{\cdot}01$ was found to be sufficient in most of the calculations presented here.

It should be pointed out that the MacCormack method and the smoothing presented in this section were also used to determine the flow field in volcanic conduits. Since both methods yielded essentially the same results when ν was adequately chosen, only the Lax–Wendroff method is reported here.

The time step in all the numerical procedures presented in this section was selected to satisfy the Courant–Friedrichs–Lewy condition for stability and convergence of finite difference schemes applied to hyperbolic equations,[32] i.e.

$$\Delta\tau \leqslant \frac{\Delta\bar{z}}{(\bar{c} + |\bar{u}|)_{\max}}, \tag{71}$$

where $\bar{c}$ denotes the nondimensional speed of sound. The space increment $\Delta\bar{z}$, or total number of grid points, was kept as a parameter in the computations to assess the sensitivity of results to the number of grid points.

All computations were performed with double precision arithmetic, and the steady-state was assumed to be achieved when the following condition

$$\sqrt{\sum_{\text{all } i} \frac{(\mathbf{U}_i^{n+1} - \mathbf{U}_i^n)^{\mathrm{T}}}{\Delta\tau} \cdot \frac{(\mathbf{U}_i^{n+1} - \mathbf{U}_i^n)}{\Delta\tau}} \leqslant 10^{-15}, \tag{72}$$

was satisfied, where the superscript T denotes transpose.

It must be noted that the finite difference methods described in the two previous sections are only valid at interior points. The boundary points were treated in two different manners. In the first manner, the method of characteristics described before was used to implement the inflow and outflow boundary conditions. This method was found to be very time consuming because of the need for interpolations

and extrapolations since the characteristics do not pass through adjacent nodes at two subsequent time steps. The second manner of implementing the boundary conditions is the one commonly used in computational fluid dynamics, i.e. (a) at a subsonic outflow, the pressure is specified and the velocity is extrapolated from the interior, (b) at a sonic outflow boundary, all the flow variables are extrapolated from the interior, and (c) at a subsonic inflow boundary, all the flow variables except for the pressure are specified, while the pressure is taken from that of the neighbour computational node.

4. INPUT DATA FOR TRANSIENT AND STEADY-STATE MAGMA ASCENT MODELLING

The four sets of input data summarized in Table I were used to model transient and steady-state magma ascent in volcanic conduits. The analytical solution of Turcotte *et al.*[13] was used to verify the accuracy of the time-dependent model presented in this paper for wave propagation phenomena in volcanic conduits without frictional and gravitational effects. The AD 79 gray and white magma eruption data of Vesuvius were employed to analyse transient and steady-state magma ascent in volcanic conduits with frictional and gravitational effects, whereas data for both basaltic fissures and the 18 May 1980 Mt St. Helens were used to compare the results obtained with the transient model presented in this paper with those from the homogeneous and non-homogeneous, steady-state models of Dobran.[3] The data presented in Table I cover a wide range of magma compositions and conduit geometries and were used to assess the validity of the transient magma ascent model presented in this paper before employing it both to the analysis of transient magma ascent in volcanic conduits and refining it to include variable magma density, and to account for the presence of crystals in magma and use improved magma viscosity laws.

5. PRESENTATION AND DISCUSSION OF RESULTS

The model equations together with the initial and boundary conditions discussed in previous sections were first solved numerically by neglecting frictional and gravitational effects so as to compare the results with the analytical solutions for transient wave propagation in volcanic conduits obtained by Turcotte *et al.*[13] Figure 3 illustrates this comparison in terms of the vent exit velocity, magma chamber pressure, and maximum dissolved water content in the magma. As seen in the figure, the numerical

Table I. Input data for the magma ascent model

	Ref 13	Vesuvius AD 79 Gray/White	Fissures	Mt. St. Helens 18 May, 1980
Friction constants, a, b	(1)	16/0·01	24/0·01	16, Figure 14
Conduit diameter D_H (m)	(1)	100	0·25–3	95
Conduit length L (km)		5	1	7
Initial magma length L_1 (km)	(1)	1	0·2	1·4
Magma chamber pres. P_0 (MPa)	(1)	132·5	27·54	185
Magma temp. T_0 (K)	1500	1120	1200	1200
Magma viscosity μ (Pa s)	(1)	(2)	100–1000	(3)
Dissolved water Y_0 (wt%)	0·2, 1, 5	3·5/4·7	1	4·6
Magma density ρ_L (kg/m^3)	2500	2550/2400	2600	2600
Mass flux G (kg/m^2 s)	(1)	$1{\cdot}91/1{\cdot}02 \times 10^4$	Figure 8	Figure 14
Atm. pressure P_{atm} (MPa)	0·1	0·1	0·1	0·1

(1) Not needed;
(2) Equation (73);
(3) Constant or Equation (73).

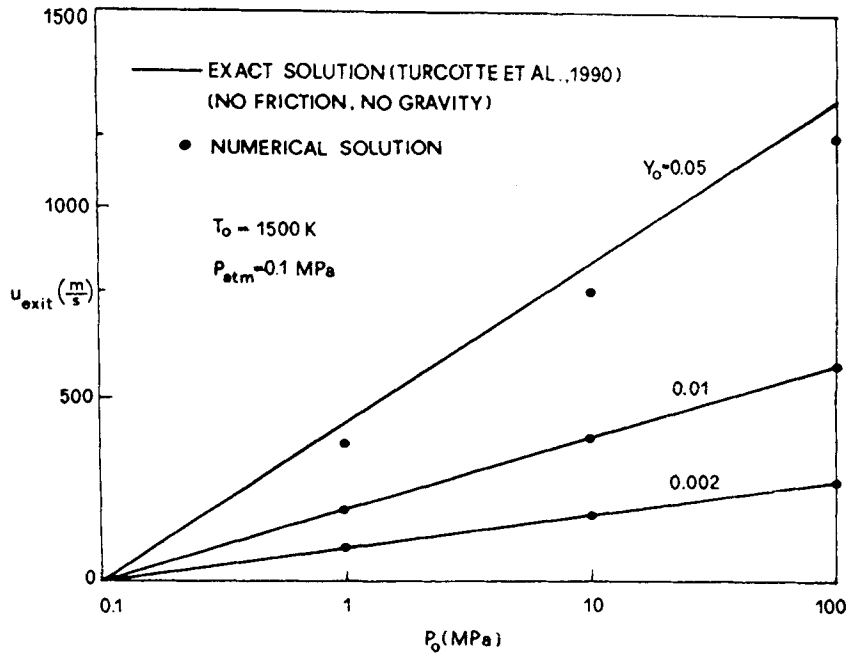

Figure 3. Comparison between the numerical results with 100 grid points and the analytical solutions of Turcotte *et al.*[13] for magma flow through conduits without frictional and gravitational effects. Shown in this figure is the exit velocity of the gas–magma mixture as a function of magma chamber pressure and dissolved water in the magma for fixed magma density, temperature, and atmospheric pressure

solution involving 100 grid points reproduces very well the analytical solution even for high values of the dissolved water in magma for which the flow gradients are high. An increase in the number of grid points to 500 produced essentially no difference between the numerical results and the analytical solution of Turcotte *et al.*[13] for all water contents shown in Figure 3.

The results corresponding to a sudden decompression of magma at 200 m above the magma chamber in a basaltic fissure 1 m wide and 1 km long are shown in Figures 4 and 5 for different numbers of grid points. Figure 4 shows the propagations of downward moving exsolution ($\alpha = 0$) and upward moving fragmentation ($\alpha = 0{\cdot}75$) fronts, and the pressure distribution in the conduit at various times. The gas volumetric fraction and the fluid velocity distributions along the conduit at different times are shown in Figure 5. The results presented in Figures 4 and 5 were obtained with a constant magma viscosity $\mu_L = 500$ Pa s, gas viscosity $\mu_G = 10^{-5}$ Pa s, and $n = 0{\cdot}7$ and $S = 6{\cdot}8 \times 10^{-8}$ Pa$^{-0{\cdot}7}$ (cf. (8)). As shown in these figures, 1000 grid points cause too much smearing due to numerical diffusion and lack of resolution, while 4000 points appear much more adequate to model the transient magma propagation from the assumed initial state. Initially, the magma moves with very steep pressure and void fraction gradients, and the flow in the volcanic conduit reaches very high velocities. These gradients and velocities decrease with time until a steady state is reached. The predicted magma propagation characteristics in the volcanic conduit presented in Figures 4 and 5 should be interpreted with great caution due to the perhaps unrealistic initial conditions used in the calculations. If such initial conditions existed in reality during the opening phases of volcanic eruptions, the ascending magma would very efficiently produce ruptures in the conduit wall and flow to the ground surface.

The results corresponding to a sudden decompression of gray magma at about 1 km above the

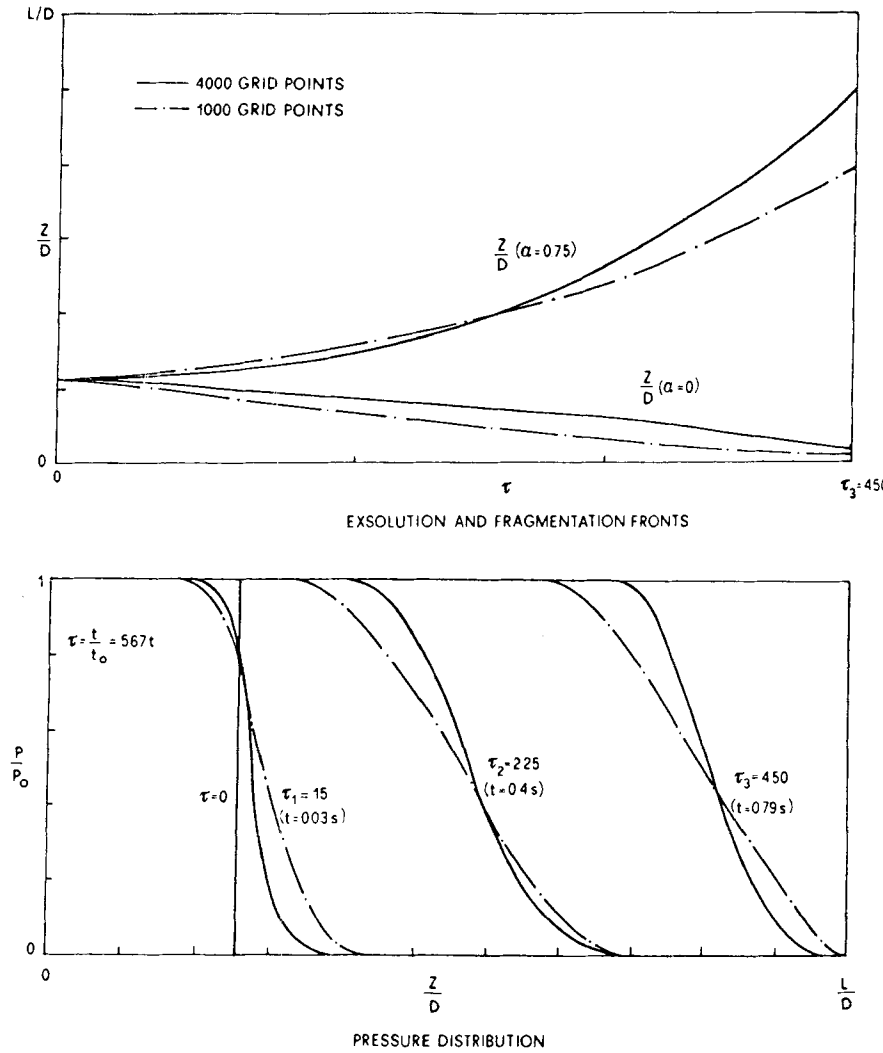

Figure 4. Propagation of exsolution and fragmentation fronts, and pressure distribution along the conduit for a 1 m wide 1 km deep basaltic fissure, with magma decompressing from about 200 m above the magma chamber. A constant magma viscosity of 500 Pa s, Henry's exsolution law (see text), and other data indicated in Table 1 were used in producing the results for different number of grid points

magma chamber of Vesuvius which is located at a depth of 5 km are illustrated in Figures 6 and 7. These figures correspond to the following magma viscosity[33]

$$\mu_L = \mu_o \exp^{-133Y}, \tag{73}$$

where $\mu_o = 2 \times 10^7$ Pa s accounts for both the anhydrous composition of the magma and the crystal content.[3] The exsolution of gray magma of Vesuvius was modelled by accounting for the gray magma composition according to Papale and Dobran[14] as

$$P > 237{\cdot}58 \times 10^5 \text{ Pa}, \quad Y = -0{\cdot}68995 \times 10^{-2} + 8{\cdot}7273 \times 10^{-10} P,$$

$$P \leqslant 237{\cdot}58 \times 10^5 \text{ Pa}, \quad Y = -4{\cdot}8747 \times 10^{-4} + 6{\cdot}0284 \times 10^{-10} P, \tag{74}$$

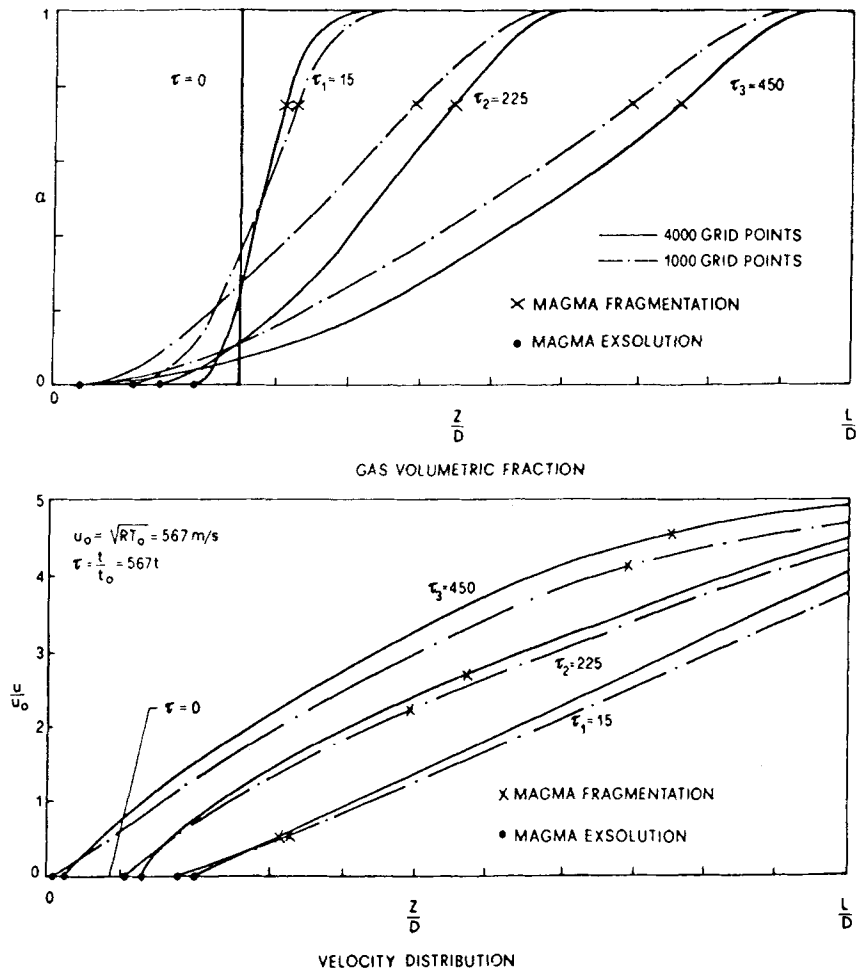

Figure 5. Gas volumetric fraction and velocity distributions along the fissure defined in Figure 4

where the pressure P is in Pa. The trends in the exsolution and fragmentation fronts, and pressure, gas volumetric fraction and velocity distributions along the volcanic conduit shown in Figures 6 and 7 are similar to those for basaltic fissures, except that the gradients are much steeper because they are caused by magma decompression at high pressure.

The transient decompression results of white magma for the AD 79 eruption of Vesuvius based on the exsolution model of Papale and Dobran[14]

$$P > 49 \times 10^6 \text{Pa}, \quad Y = -0{\cdot}022686 + 1{\cdot}0421 \times 10^{-9} P,$$

$$24{\cdot}595 \times 10^6 < P \leq 49 \times 10^6 \text{Pa}, \quad Y = -0{\cdot}0071891 + 7{\cdot}263 \times 10^{-10} P,$$

$$P \leqslant 24{\cdot}595 \times 10^6 \text{Pa}, \quad Y = -4{\cdot}3114 \times 10^{-4} + 4{\cdot}5153 \times 10^{-10} P, \tag{75}$$

differ very little from those of the gray magma decompression shown in Figures 6 and 7 and are not reported in this paper. In general, the white magma decompresses slightly slower probably due to its higher dissolved water content.

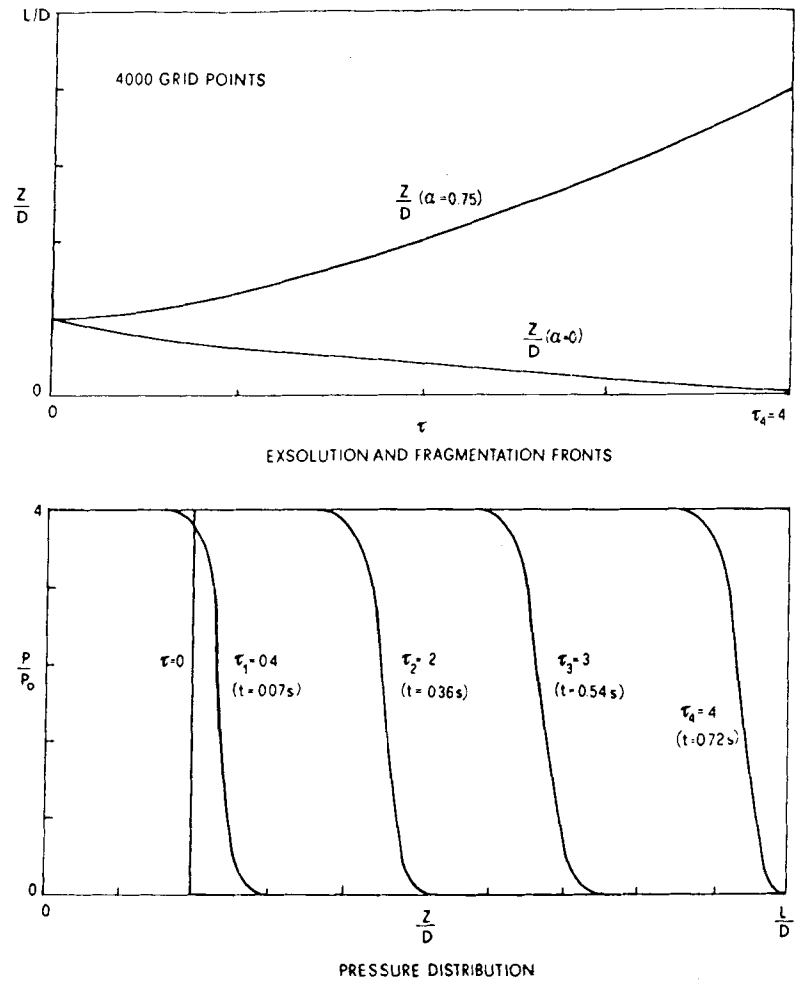

Figure 6. Propagation of exsolution and fragmentation fronts, and pressure distribution along the 5 km long volcanic conduit of Vesuvius, with gray magma decompressing from about 1 km above the magma chamber. The magma viscosity was modelled according to Shaw, [33] while the gas exsolution was modelled according to Papale and Dobran.[14] Other data used in the model are given in Table 1

The results presented in Figures 3–7 were obtained with the TVD finite difference method. It was found that an artificial viscosity of $\nu = 0{\cdot}01$ in the Lax–Wendroff method yielded comparable results to those shown in Figures 3–7 away from the shock front, while, at the front, the differences between the results of the TVD finite difference and Lax–Wendroff methods were as large as 7·23 per cent in the L_∞ norm. These differences are undoubtedly due to the use of a constant artificial viscosity in the Lax–Wendroff method employed in this paper, while the artificial viscosity of the TVD finite difference method is controlled by the flux limiter. Furthermore, it is important to indicate that the Lax–Wendroff method yielded much smoother shock fronts than the TVD scheme. Note that the artificial viscosity of the Lax–Wendroff method employed in this paper is controlled by the shock front where the flow gradients are largest.

The method of characteristics presented in this paper did not capture well the analytical wave propagation reported by Turcotte *et al.*[13] In fact, this method predicted smoother shock fronts than the TVD algorithm. This result was somewhat expected since the method of characteristics employed in

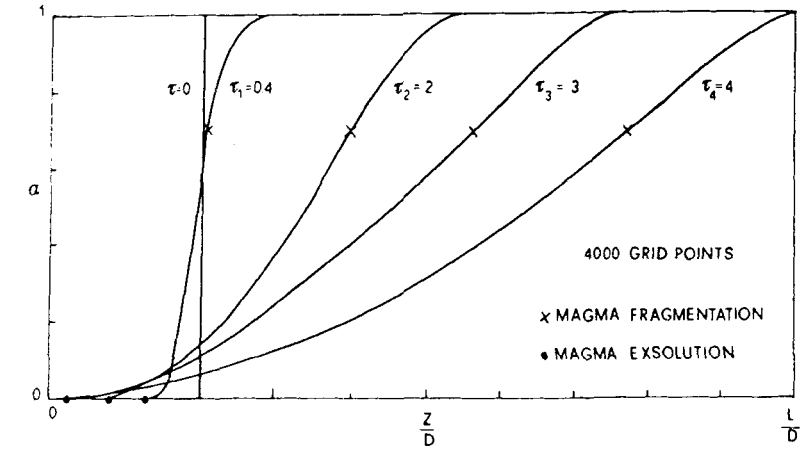

GAS VOLUMETRIC FRACTION DISTRIBUTION

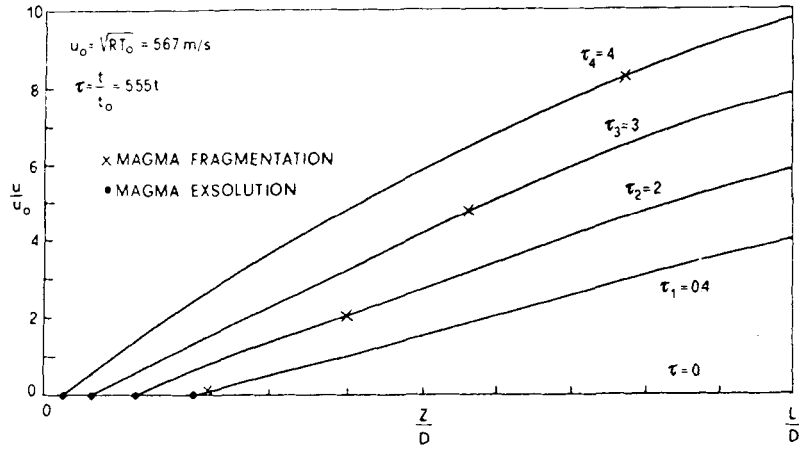

VELOCITY DISTRIBUTION

Figure 7. Gas volumetric fraction and velocity distributions along the volcanic conduit of Vesuvius defined in Figure 6.

this paper is non-conservative. The differences between the results of the TVD algorithm and those of the method of characteristics were as large as 5·78 in the L_∞ norm.

In view of these results, the computations reported next were performed with the TVD finite difference method.

The transient model of magma ascent in volcanic conduits also predicts the steady-state distributions of pressure, gas volumetric fraction, velocity, etc., after the transient period of flow development. Figures 8–14 illustrate this prediction for different conduit geometries and magma compositions, and a comparison with the results of both the homogeneous and the nonhomogeneous, steady-state, two-phase flow magma ascent models of Dobran.[3] The results for basaltic fissures shown in Figures 8–12 show that the two homogeneous models are in very good agreement for different magma viscosities and fissure widths, and that the predictions of these two models disagree with those of the non-homogeneous model for the smaller fissure widths and larger magma viscosities considered here. The steady-state, non-homogeneous, two-phase flow model of Dobran[3] accounts for slip, i.e. the relative velocity between the exsolved gas and the magma; this slip may be considerable above the magma fragmentation level in the volcanic conduit.

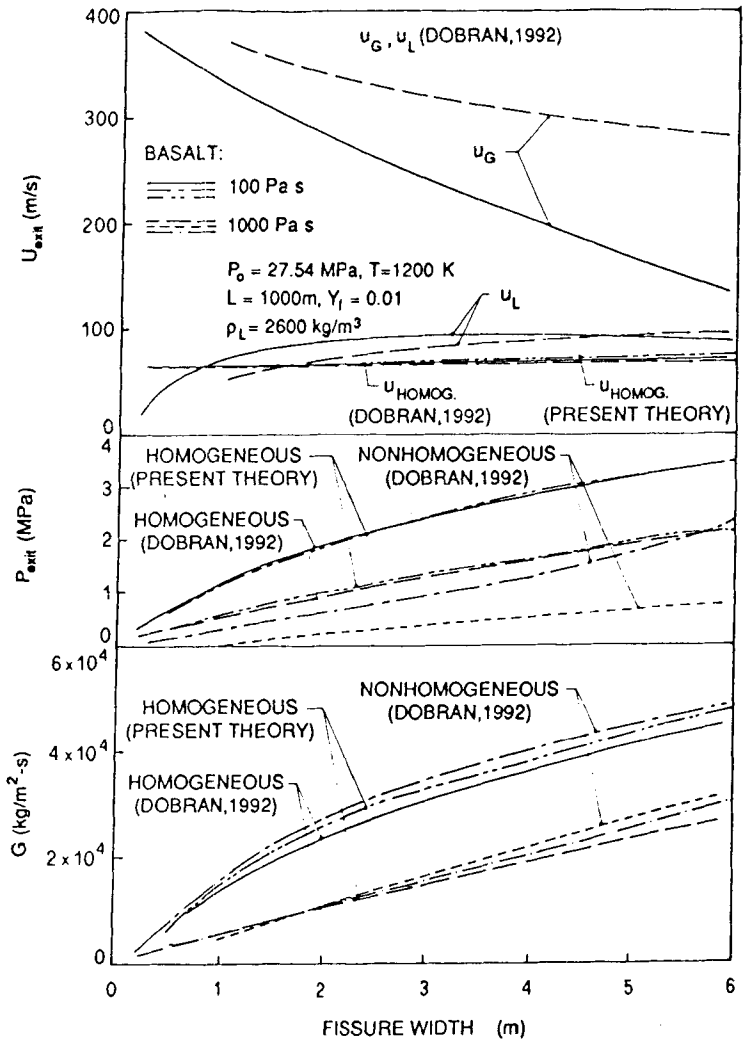

Figure 8. Distributions of critical discharge rates and exit pressures and velocities for fissures of different widths and magma viscosities, obtained by the homogeneous and non-homogeneous models. Other data used in the model are given in Table 1

Figures 13 and 14 show comparisons between the pressures and gas volumetric fractions obtained with the present transient model and those of the non-homogeneous, steady-state model of Dobran[3] for the gray and white magma eruptions of Vesuvius in AD 79 and Mt. St. Helens on 18 May 1980 respectively. As seen from these figures, the comparisons between the results of the two models are very good for a wide range of parameters of these explosive volcanic eruptions. The magma viscosity was modelled according to (73), whereas the exsolution was modelled according to (8) with $n = 0{\cdot}5$ and $S = 4{\cdot}1 \times 10^{-6}$ Pa$^{-0{\cdot}5}$ for the Mt. St. Helens and (74) and (75) for Vesuvius.

The results presented in Figures 4–7 indicate that the decompression of different magmas in various types of volcanic conduits occurs very fast with shock waves traveling through the conduit in less than a second. The accuracy of this prediction depends on the exsolution kinetics; if the flow residence time is much larger than that associated with the exsolution of dissolved gases, the accuracy of the results presented in Figures 4–7 may be very good. Note that Henry's law was employed to determine the dissolved gas mass fraction, and that this law is strictly valid when interfacial mass transfer phenomena

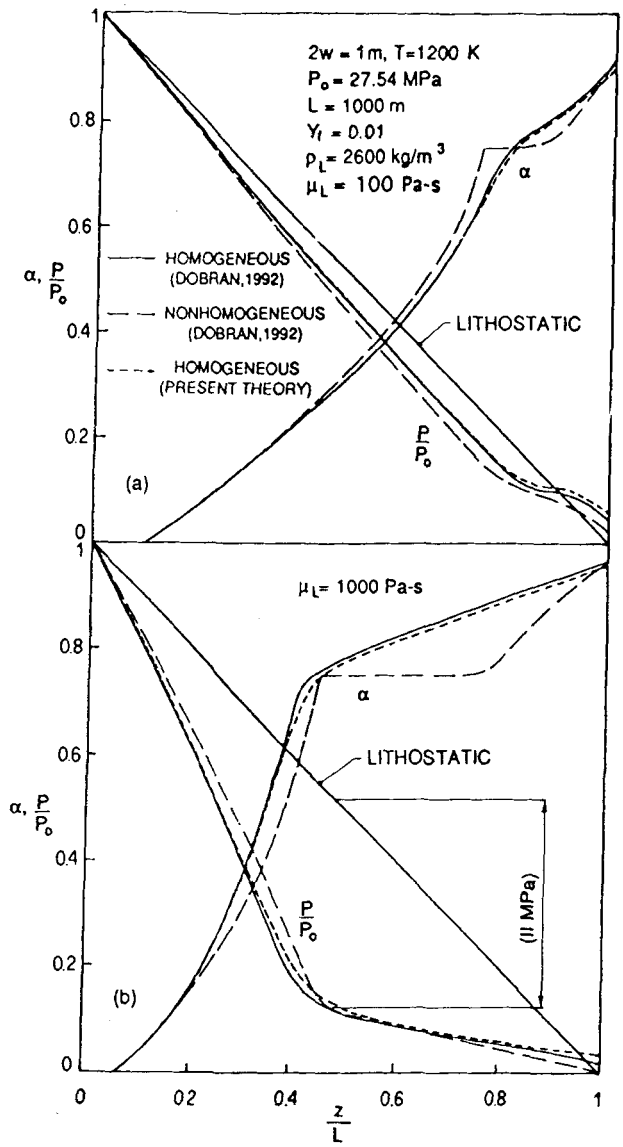

Figure 9. Distributions of volumetric fraction and pressure along a fissure 1 m wide and comparison with the results of steady-state homogeneous and non-homogeneous models. (a) Magma viscosity is 100 Pa s, and (b) Magma viscosity is 1000 Pa s

are much faster than fluid dynamic processes. Clearly, future efforts in gas exsolution modelling should address the effects of time on the exsolution of different magmatic gases from different magma compositions at different temperatures. It should also be noted that the assumed magma decompression from the initial state depicted in Figure 1 is probably not very realistic. Magma probably channels its way through the surface by slowly opening fractures until the pressure increase due to the exsolution of magmatic gas is sufficient to produce an 'explosive' opening of the volcanic conduit. A particular choice of the initial state of magma in a volcanic conduit is clearly unimportant if we are only interested in steady-state flow. The initial conditions used in this paper and shown in Figure 1 serve to both initiate the transient magma flow and test the numerical algorithm.

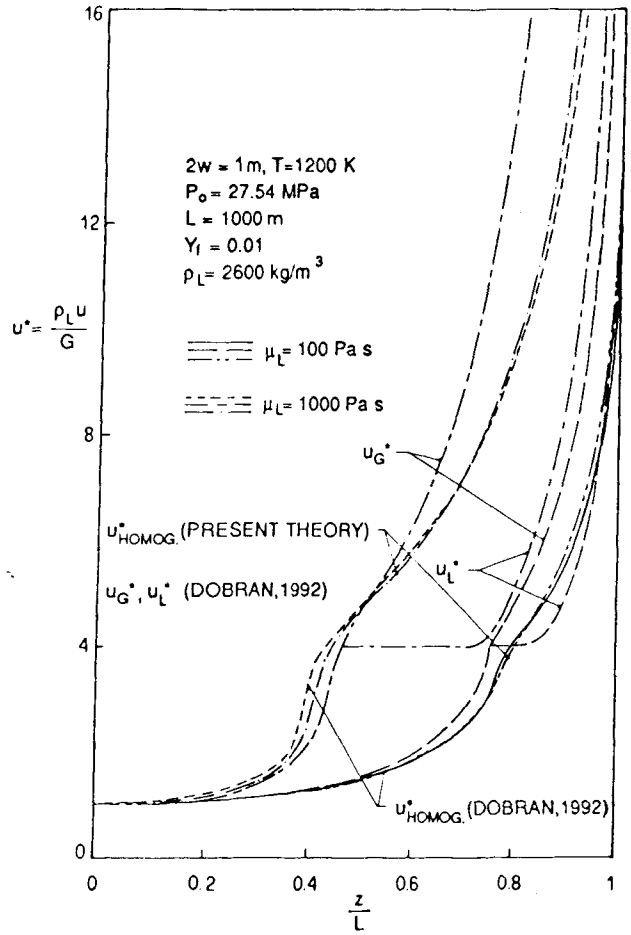

Figure 10. Distributions of velocities along a fissure 1 m wide for different magma viscosities and comparison with the results of steady-state homogeneous and non-homogeneous models

An important assumption in the model presented in this paper is that during the transient magma ascent, the volcanic conduit inlet conditions remain unchanged. In reality, this cannot be the case but may be approximated under certain conditions depending on the magma chamber geometry and the thermofluid-dynamic phenomena. When magma decompresses in a volcanic conduit, a downward moving wave enters into the magma chamber and may modify its thermofluid-dynamic conditions which in turn affect the conduit inlet conditions. A similar situation occurs at the conduit exit where the volcanic column developing above the vent may affect the magma flow conditions in the conduit, if the flow at the conduit exit is not choked. A realistic transient model of magma ascent in volcanic conduits should, therefore, account for the magma chamber, the volcanic conduit, and, possibly, the volcanic column. Such modelling is very complicated and constitutes a significant part of a project on global models of volcanoes.[25]

The agreement between the predictions of the steady state flow obtained with the transient, homogeneous, two-phase flow model presented in this paper and those of the homogeneous, steady-state, magma model of Dobran[3] provides an important validation of both models, since the physical equations were solved by different numerical procedures. (Dobran[3] used a stiff integrator for initial value problems and a shooting technique). The slight differences between the results predicted by these

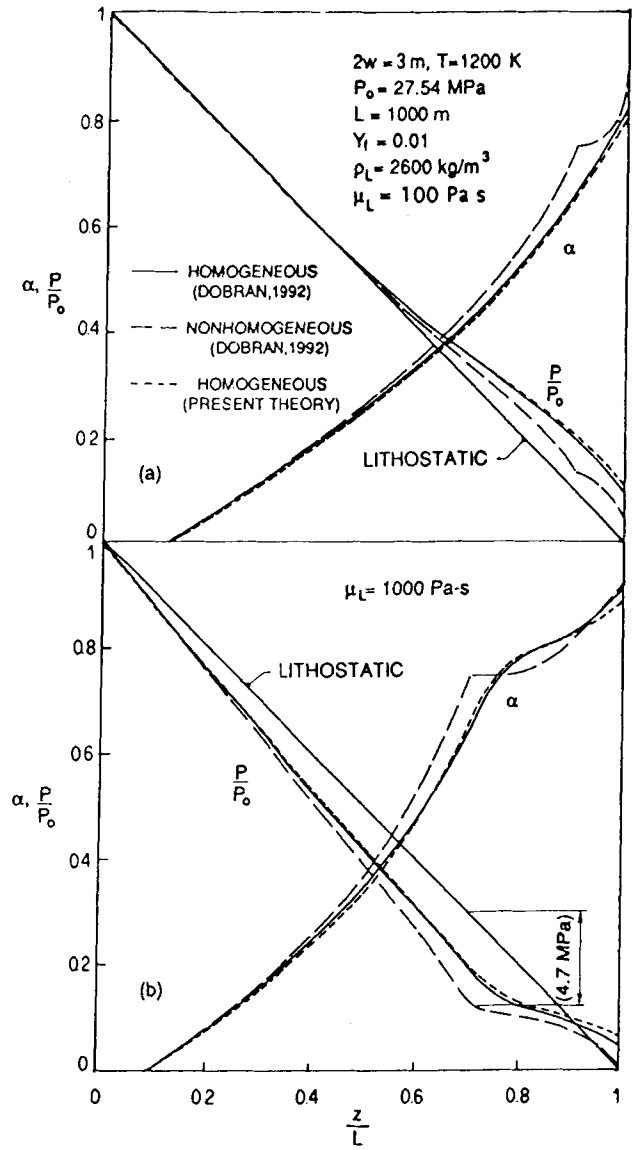

Figure 11. Distributions of gas volumetric fraction and pressure along a fissure 3 m wide and comparison with the results of steady-state homogeneous and non-homogeneous models. (a) Magma viscosity is 100 Pa s, and (b) magma viscosity is 1000 Pa s

two homogeneous models (cf. Figures 8–12) may be due to the errors of the two numerical algorithms and the different number of grid points as well as to the approximate procedure used by Dobran[3] in his non-homogeneous model to force the flow to behave homogeneously. Such a procedure consisted of taking a very high interfacial drag coefficient between the gas and the magma which prevented the relative motion between the phases. The differences between the results predicted by the homogeneous, time-dependent model presented in this paper and the steady-state, non-homogeneous or velocity slip model of Dobran[3] shown in Figures 8–14 clearly show the importance of non-equilibrium effects in volcanic conduits above the magma fragmentation level where the gas and pyroclasts accelerate

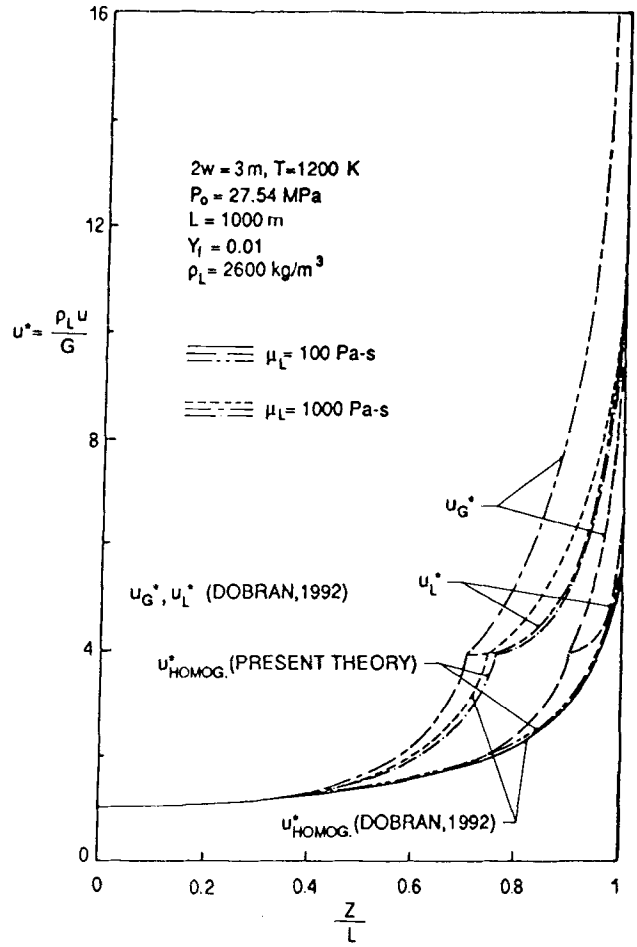

Figure 12. Distributions of velocities along a fissure 3 m wide for different magma viscosities and comparison with the results of steady-state homogeneous and non-homogeneous models

differently. Such differential acceleration produces large velocity differences at the exit of the conduit for large size pyroclasts. In particular, the pressure and gas void fraction distributions along the conduit predicted by the homogeneous and non-homogeneous models agree rather closely with each other for pyroclasts sizes of up to 100 μm.

6. CONCLUSIONS

A one-dimensional, time-dependent, isothermal, homogeneous, two-phase flow model was developed to study magma ascent in volcanic conduits. At each grid point, the physical modelling equations were solved explicitly by means of a TVD predictor–corrector method and a predictor–corrector tecnique based on the method of characteristics. The numerical solutions were verified by comparisons with an analytical solution for wave propagation without friction and gravity in volcanic conduits, and with the predictions of a homogeneous, two-phase, steady state model of magma ascent for different volcanic conduit diameters and lengths and magma compositions.

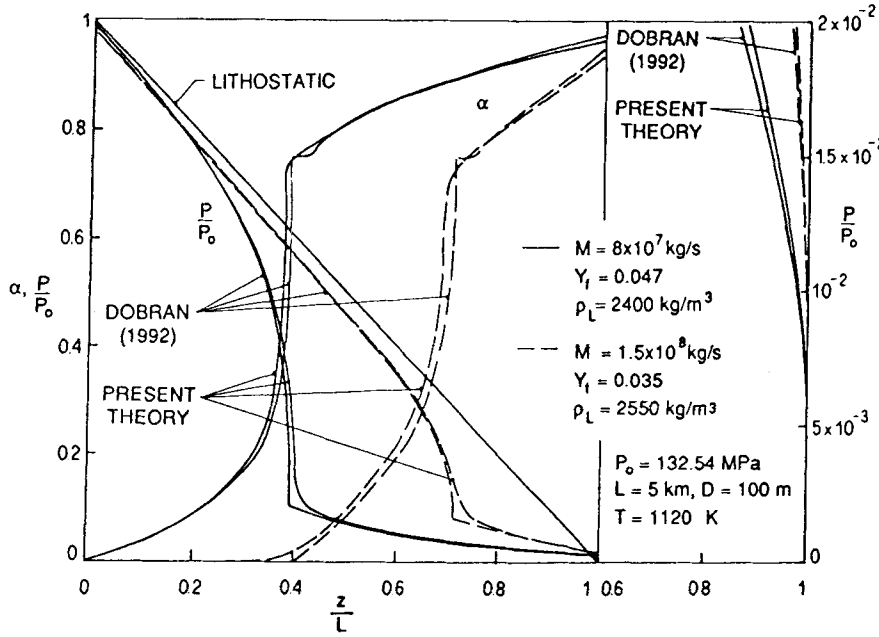

Figure 13. Gas volumetric fraction and pressure distributions from present and previous steady-state models of magma ascent along the 5 km long and 100 m diameter conduit for the eruption of Vesuvius in AD 79 as functions of the discharge rate, water content, and magma density for white and gray magmas

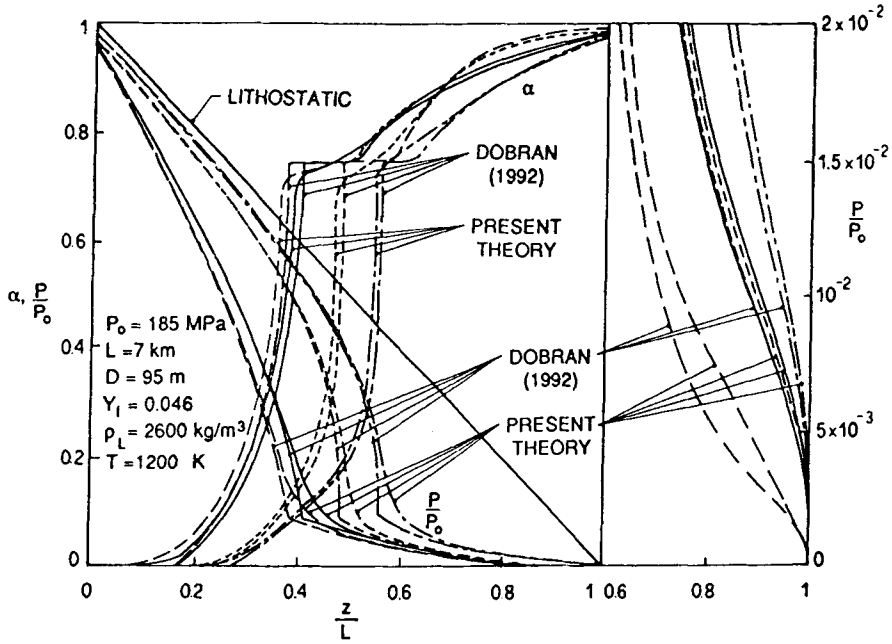

Figure 14. Gas volumetric fraction and pressure distributions from present and previous steady-state models of magma ascent along the 7 km long and 95 m diameter conduit for the Mt St. Helens eruption on 18 May 18 1980. The results show the effects of critical discharge rates, constant and variable magma viscosities, and different values of the friction loss coefficient b. $G = 6208$ kg/m^2 s: $\mu_L = \text{const.}$, $b = 0{\cdot}01$; $\mu_0 = \text{const.}$, $b = 0{\cdot}01$; $\mu_0 = \text{const.}$, $b = 0{\cdot}1$. $G = 2160$ kg/m^2 s: $\mu_L = \text{const.}$, $b = 0{\cdot}01$.

The results from the transient magma ascent model were found to reproduce very well the analytical solutions of wave propagation in volcanic conduits without friction and gravitational effects, and with previous steady state, homogeneous magma ascent models in fissures and volcanic conduits with frictional and gravitational effects. When the transient model was applied to the decompression of magma in fissures and conduits, very steep flow gradients were found with an exsolution front propagating downward toward the magma chamber, and fragmentation and shock wave fronts propagating upward toward the conduit exit. The magma decompression results showed very short times of front propagation through the conduits and indicate the need for incorporating kinetic effects into the gas exsolution model. A realistic transient magma ascent model requires the coupling of the conduit model with a transient magma chamber model and, possibly, with a pyroclastic dispersion model above the vent to model correctly the wave propagation through the volcanic conduit and the coupling between phenomena occurring in the magma chamber, conduit and volcanic column. Such a physical modelling approach, coupled with future model-oriented volcanological, geophysical, petrological, etc., data should lead to the development of global volcanic simulators and more realistic volcanic hazard assessments.

ACKNOWLEDGEMENTS

This work was partly supported by the Gruppo Nazionale per la Vulcanologia of Italy, and by the Commission of the European Communities under Contract. No. EV5V-CT92-0190. The author is grateful to Dr Flavio Dobran for his help during the course of the research presented in this paper.

REFERENCES

1. G. A. Macdonald, *Volcanoes*, Prentice Hall, Englewood Cliffs, N.J., 1972.
2. R. S. J. Sparks, 'The dynamics of bubble formation and growth in magmas: A review and analysis', *J. Volcanol. Geotherm. Res.*, **3**, 1–37 (1978).
3. F. Dobran, 'Nonequilibrium flow in volcanic conduits and application to the eruptions of Mt. St. Helens on May 18, 1980, and Vesuvius in AD 79', *J. Volcanol. Geotherm. Res.*, **49**, 285–311 (1992).
4. F. Dobran and P. Papale, 'Magma-water interaction in closed systems and application to lava tunnels and volcanic conduits', *J. Geophys. Res.*, **98**, 14041–14058 (1993).
5. F. Barberi, J. M. Navarro, M. Rosi, R. Santacroce and A. Sbrana, 'Explosive interaction of magma with ground water: Insight from xenoliths and geothermal drillings', *Rendiconti Soc. Ital. Miner. Petrol.*, **43**, 901–926 (1988).
6. S. W. Kieffer, 'Sound speed in liquid-gas mixtures: Water-air and water-steam', *J. Geophys. Res.*, **82**, 895–904 (1977).
7. S. I. Pai, Y. Hsu and J. A. O'Keefe, 'Similar explosive eruptions of lunar and terrestrial volcanoes', in *Proc. 9th Lunar Planet. Sci. Conf.*, pp. 1485–1508, 1978.
8. J. Wilson and J. W. Head III, 'Ascent and eruption of basaltic magma on the earth and moon', *J. Geophys. Res.*, **86**, 2971–3001 (1981).
9. L. Wilson, R. S. J. Sparks and G. P. L. Walker, 'Explosive volcanic eruptions, IV. The control of magma properties and conduit geometry on eruption column behavior', *Geophys. J. Roy. Astron. Soc.*, **63**, 117–148 (1980).
10. S. Vergniolle and C. Jaupart, 'Separated two-phase flow and basaltic eruptions', *J. Geophys. Res.*, **91**, 12842–12860 (1986).
11. G. Buresti and C. Casarosa, 'One-dimensional adiabatic flow of equilibrium gas-particle mixtures in long vertical ducts with friction', *J. Fluid Mech.*, **203**, 251–272 (1989).
12. G. Giberti and L. Wilson, 'The influence of geometry on the ascent of magma in open fissures', *Bull. Volcanol.*, **52**, 515–521 (1990).
13. D. L. Turcotte, D. L., H. Ockendon, J.R. Ockendon and S.J. Cowley, 'A mathematical model of vulcanian eruptions', *Geophys. J. Int.*, **103**, 211–217 (1990).
14. P. Papale and F. Dobran, 'Modeling of the ascent of magma during the plinian eruption of Vesuvius in AD 79', *J. Volcanol. Geotherm. Res.*, in press, 1994.
15. P. Papale and F. Dobran, 'Magma flow along the volcanic conduit during the plinian and pyroclastic flow phases of the May 18, 1980 Mt. St. Helens eruption', *J. Geophys. Res.*, in press, 1994.
16. G. Macedonio, F. Dobran and A. Neri, 'Erosion processes in volcanic conduits and an application to the AD 79 eruption of Vesuvius', *Earth. Planet. Sci. Let.*, in press, 1994.
17. F. Dobran, F., A. Neri and M. Todesco, 'Pyroclastic flow hazard at Vesuvius', *Nature*, in press, 1994.
18. F. J. Spera, D. A. Yuen, J. C. Greer and G. Sewell, 'Dynamics of magma withdrawal from stratified magma chambers', *Geology*, **14**, 723–726 (1986).

19. M. F. Sheridan and K. H. Wohletz, 'Hydrovolcanism: Basic considerations and review', *J. Volcanol. Geotherm. Res.*, **17**, 1–29 (1983).
20. G. A. Valentine K. H. Wohletz and S. W. Kieffer, 'Sources of unsteady column dynamics in pyroclastic flow eruptions', *J. Geophys. Res.*, **96**, 21887–21892 (1991).
21. F. Dobran, A. Neri and G. Macedonio, 'Numerical simulation of collapsing volcanic columns', *J. Geophys. Res.*, **98**, 14041–14058 (1993).
22. A. Neri and F. Dobran, 'Influence of eruption parameters on the dynamics and thermodynamics of collapsing volcanic columns', submitted, 1995.
23. S. Self, L. Wilson and I. A. Nairn, 'Vulcanian eruption mechanisms', *Nature*, **277**, 440–443 (1979).
24. S. W. Kieffer and B. Sturtevant, 'Laboratory studies of volcanic jets', *J. Geophys. Res.*, **89**, 8253–8268 (1984).
25. F. Dobran, *Global Volcanic Simulation of Vesuvius*, CNR-GNV Report, Giardini, Pisa, 1993.
26. G. B. Wallis, *One-Dimensional Two-Phase Flow*, McGraw-Hill, New York, 1969.
27. B. Gabutti, 'On two upwind finite-difference schemes for hyperbolic equations in non-conservation form', *Computer and Fluids*, **10**, 207–230 (1983).
28. E. Isaacson and H. B. Keller, *Analysis of Numerical Methods*, John Wiley & Sons, New York, 1966.
29. C. A. J. Fletcher, *Computational Techniques for Fluid Dynamics, Volume II*, Springer-Verlag, New York, 1991.
30. R. W. MacCormack, 'The effect of viscosity in hypervelocity impact cratering', *AIAA Paper No. 69-354*, 1969.
31. S. F. Davis, 'A simplified TVD finite difference scheme via artificial viscosity', *SIAM J. Sci. and Statist. Comput.*, **8**, 1–18 (1987).
32. M. Holt, *Numerical Methods in Fluid Dynamics*, 2nd ed., Springer-Verlag, New York, 1984.
33. H. R. Shaw, 'Rheology of basalt in the melting range', *J. Petrol.*, **10**, 510–535 (1969).